

# SrRuO<sub>3</sub> Growth on DyScO<sub>3</sub> Using Soft-Lithographic Patterning and Pulsed Laser Deposition

---

*Bachelor thesis*

**The Inorganic Materials Science Group**

**University of Twente**

Committee:

Chairperson: André ten Elshof

Supervisor: Maarten Nijland

External examiner: Jaap Flokstra

Member: Gert-Jan Koster

By Cristian Deenen

09-09-2014

## Abstract

In this project SrRuO<sub>3</sub> growth on DyScO<sub>3</sub> was researched. Using soft elastomeric PDMS stamps a ZnO mask was patterned upon which a SrRuO<sub>3</sub> layer was deposited using pulsed laser deposition. The ZnO line pattern was etched away using a 0.01wt% HCl solution. The resulting nanowires were around 6 nm high and conducted electricity over a few hundred micrometer. These nanowires were used to research the homo- and heteroepitaxial growth mechanics of SrRuO<sub>3</sub>.

When SrRuO<sub>3</sub> was deposited on single terminated DyScO<sub>3</sub> with no mask, it grew into a thin film with trenches. On top of the ZnO mask the SrRuO<sub>3</sub> grew into a rough film, probably due to the different growth directions of the islands. In between the ZnO mask, no consistent growth was found.

After the mask was removed, a second and third SrRuO<sub>3</sub> layer were deposited to further investigate the growth mechanics. The new SrRuO<sub>3</sub> layers grew on the DyScO<sub>3</sub> in between the nanowires and in varying degrees on top of the SrRuO<sub>3</sub> nanowires. When the second or third layer was grown on a smooth film, the new layer would also grow as a smooth film, and when it was grown on islands the new layer would also grow islands. The growth seemed to continue the growth mechanism of the surface on which it was deposited.

The method that was used gave inconsistent results, with many attempts that failed either during the mask production or during the SrRuO<sub>3</sub> deposition. Therefore it was impossible to draw firm conclusions about the growth mechanics.

# Table of contents

<b>1</b>	<b>Introduction</b> .....	<b>4</b>
<b>2</b>	<b>Perovskite crystals</b> .....	<b>5</b>
2.1	Structure and properties .....	5
2.1.1	Structure.....	5
2.1.2	DyScO <sub>3</sub> and SrRuO <sub>3</sub> .....	5
2.2	Crystal growth theory .....	6
2.3	Crystal growth using PLD.....	7
<b>3</b>	<b>Fabrication and characterization</b> .....	<b>8</b>
3.1	DyScO <sub>3</sub> substrate treatment.....	8
3.2	ZnO mask fabrication .....	8
3.3	PLD growth of SrRuO <sub>3</sub> nanowires .....	9
<b>4</b>	<b>Results and discussion</b> .....	<b>11</b>
4.1	DyScO <sub>3</sub> substrate treatment.....	11
4.2	SrRuO <sub>3</sub> growth on DyScO <sub>3</sub> .....	12
4.3	ZnO mask fabrication on Si.....	13
4.4	ZnO mask fabrication on DyScO <sub>3</sub> .....	14
4.5	Growth of SrRuO <sub>3</sub> on the ZnO mask.....	15
4.6	Second and third SrRuO <sub>3</sub> deposition.....	18
4.7	Electrical analysis of the SrRuO <sub>3</sub> nanowires .....	20
<b>5</b>	<b>Conclusion and recommendations</b> .....	<b>21</b>
<b>6</b>	<b>Acknowledgements</b> .....	<b>22</b>
<b>7</b>	<b>References</b> .....	<b>23</b>

# 1 Introduction

The perovskite class of materials has a large range of interesting properties, such as superconductivity [1], ferromagnetism [2] and ferroelectricity [3]. One of these perovskites is SrRuO<sub>3</sub>. SrRuO<sub>3</sub> has gained interest because of its ability to conduct electricity, which is regularly used for bottom electrodes [4]. Since it is chemically and thermally stable, SrRuO<sub>3</sub> structures can be fabricated at modest temperatures, which makes it easy to work with and increases the range of applications for which it can be used. The lattice constant of SrRuO<sub>3</sub> is very close to several different perovskite materials such as DyScO<sub>3</sub>, which should lead to heteroepitaxial growth with minimal strain. SrRuO<sub>3</sub> epitaxy is very sensitive to the chemical nature of terminations, which can be used to grow self-organized nanowires on DyScO<sub>3</sub>, as a previous study by Kuiper *et al.* shows [5].

Kuiper shows that SrRuO<sub>3</sub> patterning is possible on DyScO<sub>3</sub>, but because the patterning depends on the surface chemistry of the substrate, it is hard to control. Since the growth mechanics of SrRuO<sub>3</sub> are still relatively unknown, a method was developed to try to give a controlled environment to research the differences between SrRuO<sub>3</sub> homo- and heteroepitaxy on DyScO<sub>3</sub>. Using soft elastomeric PDMS stamps, a ZnO mask was created. After growing a SrRuO<sub>3</sub> thin film using pulsed laser deposition the ZnO mask was removed in a diluted acid. Patterned lines of SrRuO<sub>3</sub> were obtained with DyScO<sub>3</sub> in between. Continued growth of SrRuO<sub>3</sub> may shed light on its growth behavior. One of the growth mechanics shown in figure 1.1 can be expected.

Two growth mechanisms can be identified. In figure 1.1a the new layer fills the space in between the nanowires, having no clear preference between homo- or heteroepitaxy. The situation in figure 1.1b would happen when the SrRuO<sub>3</sub> shows a clear preference for homoepitaxy. A combination of the two mechanisms is also possible.

This study shows that the used method does not lead to full control over SrRuO<sub>3</sub> nanowire production. This is due to problems with the mask fabrication and uncontrolled SrRuO<sub>3</sub> growth. The deposition of SrRuO<sub>3</sub> on top of DyScO<sub>3</sub> was expected to result in almost single-crystalline, atomically smooth thin films, but this was not always the case. The small amount of samples that were successfully made showed varied growth mechanics from which little conclusions could be drawn. Combinations of both homo- and heteroepitaxy were observed.

In chapter 2 the background information on perovskites and crystal growth are given. Chapter 3 discusses the method for making SrRuO<sub>3</sub> nanowires. The experimental results are given in chapter 4. The conclusion and recommendations can be found in chapter 5.

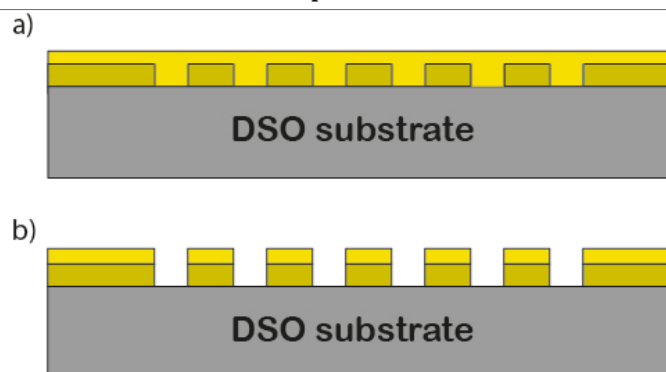


**Figure 1.1** A schematic illustration of two possible growths of a second SrRuO<sub>3</sub> layer (bright yellow). (a) The new layer fills the empty spaces in between the structures. (b) The new layer grows on top of the structures.

## 2 Perovskite crystals

### 2.1 Structure and properties

#### 2.1.1 Structure

$\text{SrRuO}_3$  and  $\text{DyScO}_3$  are perovskites in the  $\text{ABO}_3$  class, which have alternating AO and  $\text{BO}_2$  layers. The structure of an ideal cubic perovskite is shown in figure 2.1.

The structure of a perovskite is determined by the size of the oxygen octahedra surrounding the B atom (see figure 2.1). The A atoms will fill the holes between the oxygen. The rules of Goldschmidt give the following conditions for the ideal relation between the different radii [6]:

$$r_A + r_O = \sqrt{2}(r_B + r_O) \quad \text{Eq. 2.1}$$

If this relation is not satisfied, the deviation can be found through the tolerance factor  $t$  [6]:

$$t = \frac{r_A + r_O}{\sqrt{2}(r_B + r_O)} \quad \text{Eq. 2.2}$$

An ideal perovskite structure is formed when equation 2.1 is satisfied, which gives  $t = 1$ . If  $t > 1$ , a polar distortion will develop because the B atom is too small for the oxygen octahedron. If  $t < 1$ , the A atom is too small compared to the space between the oxygen octahedra, in which case the A atom cannot effectively bond with the O atoms. The oxygen octahedra will rotate and tilt if  $t$  is only slightly smaller than 1.

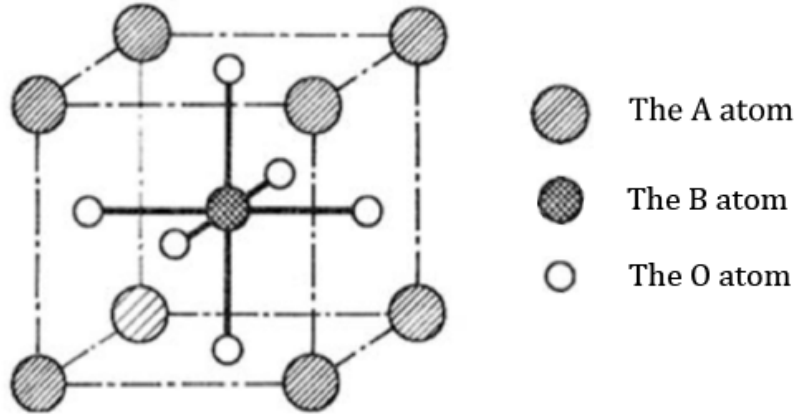


Figure 2.1 A schematic illustration of the ideal cubic perovskite structure. [6]

The (pseudo-)cubic lattice constant of the unit cell can in this case be calculated from the lattice parameters using equation 2.3 [7].

$$a_p = \frac{1}{2}\sqrt{a^2 + b^2} \approx \frac{c}{2} \quad \text{Eq. 2.3}$$

#### 2.1.2 $\text{DyScO}_3$ and $\text{SrRuO}_3$

$\text{DyScO}_3$  was used as substrate for this project. As received,  $\text{DyScO}_3$  substrates were double terminated with an alternating  $\text{DyO}^+$  and  $\text{ScO}_2^-$  layer. The lattice parameters of  $\text{DyScO}_3$  are  $a = 5.560 \text{ \AA}$ ,  $b = 5.561 \text{ \AA}$  and  $c = 7.903 \text{ \AA}$ , giving a pseudo-cubic lattice constant of  $3.932 \text{ \AA}$ . From equation 2.2 the tolerance factor can be calculated as 0.767.

SrRuO<sub>3</sub> has lattice parameters  $a = 5.5670 \text{ \AA}$ ,  $b = 5.5304 \text{ \AA}$  and  $c = 7.8446 \text{ \AA}$  [4], and using equation 2.3 we find a lattice constant of  $a_p = 3.9235 \text{ \AA}$ . This lattice constant is almost identical to the lattice constant of DyScO<sub>3</sub> of  $3.932 \text{ \AA}$ . This results in nearly strain free epitaxial growth, making DyScO<sub>3</sub> a good candidate to grow SrRuO<sub>3</sub> on.

The goldsmith relation (equation 2.1) is almost satisfied for SrRuO<sub>3</sub>, with a tolerance factor  $t = 0.993$ . Because of this tolerance factor, it is known that the crystal has some polar distortion, since the Sr atom is slightly too small for the oxygen octahedron.

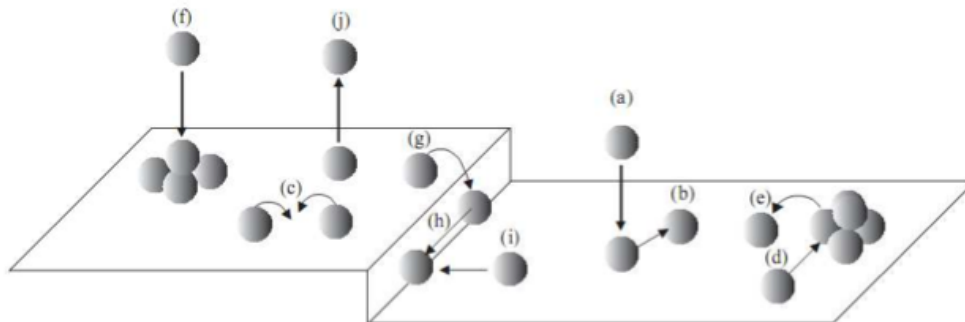


**Figure 2.2** Schematic illustration of the surface of a crystal. Atoms and molecules can stick to the surface (a, f), diffuse (b), form islands (c, d), detach from islands (e), step up or down terraces (g) and detach from the surface (j). [9]

## 2.2 Crystal growth theory

Using pulsed laser deposition it is possible to grow crystals a monolayer at a time. Single atoms or molecules will land on the substrate surface, on which they can diffuse and form islands. Due to the miscut angle of a crystal, the surface consists of terraces with a height separation of unit cell height. The movements of the single atoms or molecules are shown in figure 2.3. Atoms or molecules can stick to the surface when they are deposited (a and f), from which they can diffuse (b) or form islands (c and d), detach from islands (e), step up or down on terrace steps (g) and detach from the surface (j).

Certain parameters that influence crystal growth can be controlled. For instance the miscut angle, ablation temperature and gas composition and pressure during ablation [9].

The film surface free energy  $\gamma_f$  and the substrate surface free energy  $\gamma_s$  distinguish two different types of growth. If  $\gamma_s < \gamma_f$  three dimensional growth occurs, which is known as Volmer-Weber growth mode, and if  $\gamma_s > \gamma_f$  two dimensional growth

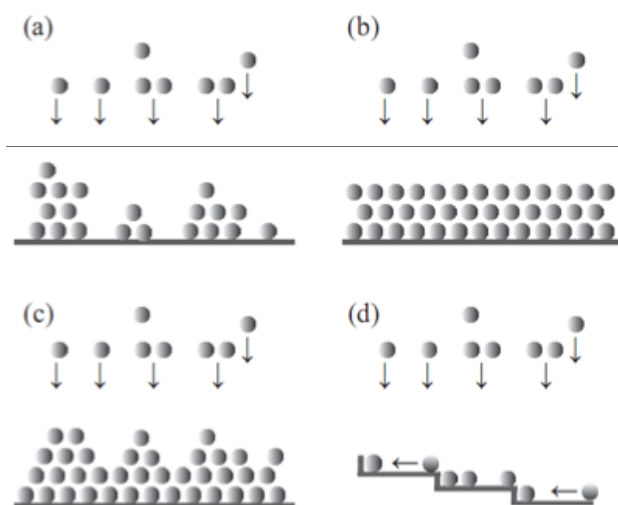


**Figure 2.3** A schematic illustration of (a) 3D island growth, Volmer-Weber, (b) 2D layer by layer growth, Frank-van der Merwe, (c) Stranski-Krastanov growth, (d) 2D step flow growth. [9]

occurs, which is known as Frank- van der Merwe growth mode. A combination of both growth modes is possible, which is called Stranski-Krastanov growth [9]. Volmer-Weber growth mode is depicted in figure 2.3a and Frank- van der Merwe growth is depicted in figure 2.3b. Stranski-Krastanov growth is depicted in figure 2.3c. The two dimensional growth can be divided into two groups, dependent on the diffusion distance [9]. If the diffusion distance is small compared to the step width, adatoms will form islands (figure 2.2c and 2.2d). If the diffusion distance is large compared to the step width the adatoms will nucleate on the terrace edges, which is called step-flow-growth (figure 2.3d). Earlier research [7] shows that  $\text{SrRuO}_3$  growth on  $\text{DyScO}_3$  is either 2D step-flow growth, island growth or a combination of the two.

### 2.3 Crystal growth using PLD

Pulsed laser deposition (PLD) is a method to grow epitaxial films. Its basic operation is based on the vaporization of material by firing a high-energy laser at a target in a vacuum chamber, for this assignment an ultra-violet (UV) laser was used. The ablated material is ejected from the target as plasma towards the substrate where a fine layer of material is collected. Due to the high energy of the UV beam the ablation plume consists mainly of atomic and diatomic particles, allowing controlled epitaxial growth of structures [10]. Controlling the pressure, temperature and gas mixture in the vacuum chamber can influence the diffusivity of the particles, and therefore influence growth. Controlling the gas mixture in the vacuum chamber can exert further control over the grow process [7]. Figure 2. is a schematic drawing of a PLD system.

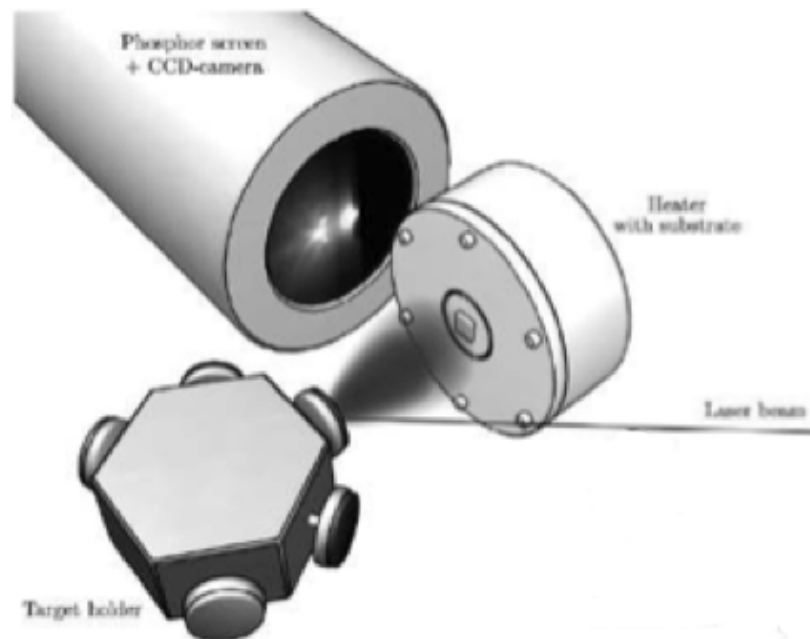


**Figure 2.4** Schematic illustration of a PLD system. The laser vaporizes the target which material lands on the substrate. [9]

## 3 Fabrication and characterization

### 3.1 DyScO<sub>3</sub> substrate treatment

Previous research [5] has shown that SrRuO<sub>3</sub> preferentially nucleates on one type of termination, so a method taken from Kleibeuker [8] was used to make the substrate single terminated. The DyScO<sub>3</sub> substrates were annealed in a tube furnace for 4 hours at 1000 °C under a 150 mL/min O<sub>2</sub> flow. A roughening step was included to increase the number of step edges, see figure 3.1a. Roughening was achieved by immersing the substrate in water for 30 minutes, and subsequently for 30 seconds in buffered HF (NH<sub>4</sub>F:HF = 87.5:12.5, pH = 5.5), in an ultrasonic bath. The substrate was rinsed three times in water and once ethanol, which was then ready for etching.

Looking at the chemistry of Dy<sub>2</sub>O<sub>3</sub> and Sc<sub>2</sub>O<sub>3</sub> we see that both materials are soluble in acidic solutions, so an acid treatment would not create a single terminated surface. However, in a NaOH solution, the reaction found in equation 3.1 occurs [11]. This shows that the dysprosium is removed by immersing the substrate in NaOH.

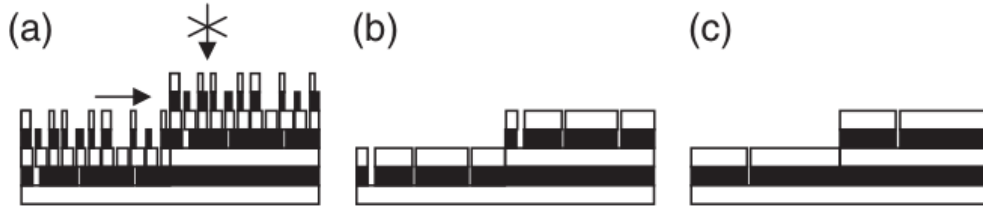
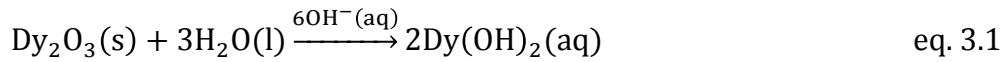


**Figure 3.1** Schematic illustration of the cross section of the DyScO<sub>3</sub> (110) top layers. Black represents the DyO and white the ScO<sub>2</sub>. (a) After surface roughening, (b) after surface roughening and selective etching, and (c) after selective alkaline etching. [8]

### 3.2 ZnO mask fabrication

The ZnO mask was created from a wet-chemical ZnO complex using soft elastomeric stamps. The ZnO complex was made by combining Zn(NO<sub>3</sub>)<sub>2</sub> and polyacrylic acid (PAA). The quality of the ZnO wires is dependent on several variables. The relative concentrations of the Zn(NO<sub>3</sub>), PAA and water and the curing time influenced the viscosity [12] and the mechanical strength of the ZnO complex [13].

A solution of 0.05g PAA (supplied by Sigma-Aldrich with M = 1800 g/mole) and 0.18g Zn(NO<sub>3</sub>)<sub>2</sub>•6H<sub>2</sub>O (supplied by Sigma-Aldrich at reagent grade purity of 98%) in 6ml water was used to create the mask. To create the soft elastomeric (PDMS) stamps, a silanized silicon master from LightSmyth with a 200 nm groove depth, 416 nm line width and period of 833.3 nm (part nr. SNS-C12-1212-200-P) was used. Using mechanical stirring, PDMS (sylgard 184 silicone elastomer kit by Dow Corning with a base and curing agent weight ratio

of 10:1) was made, which was then cured on top of the master. After the PDMS was cured the stamp was cut in 9 pieces slightly smaller than 5x5mm. The smaller stamps and the DyScO<sub>3</sub> substrate were then cleaned in a plasma cleaner (Harrick) for 5 minutes at 35 W, pumped down with a diaphragm pump. A 30  $\mu$ L drop of the ZnO complex was applied to the stamp and spread evenly using a spincoater (Laurel, model nr. WS-400B-6NPP/lite/as/ond), following the program shown in table 3.1, with an acceleration of 27.5 R/s<sup>2</sup>. This left a thin layer of the ZnO complex on the PDMS stamp (figure 3.2a). The stamp was applied to the substrate (figure 3.2b), which was hardened for an hour at 90 °C on a hot plate after which the stamp was removed from the substrate, leaving a substrate with the desired structure (figure 3.2c).

The substrate was cleaned in an ultrasonic bath for 30 seconds, and annealed in a microwave oven (Milestone MicroSynth) following the program shown in table 3.2, using only linear temperature changes. During annealing the PAA evaporated, leaving behind the ZnO mask.

Table 3.1: Spincoater program

Time (s)	RPM
15	500
5	1000
180	5000
15	500

Table 3.2: Microwave program

Time (mins)	Starting Temp (°C)	Ending Temp (°C)
15	0	400
15	400	400
8	400	600
32	600	600

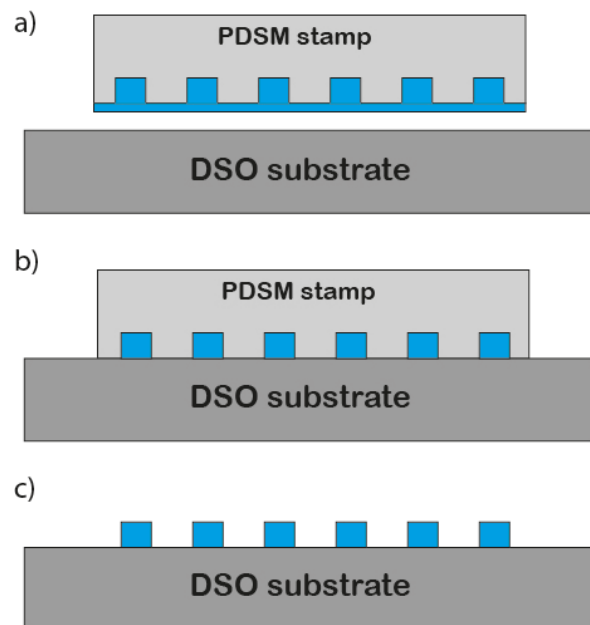
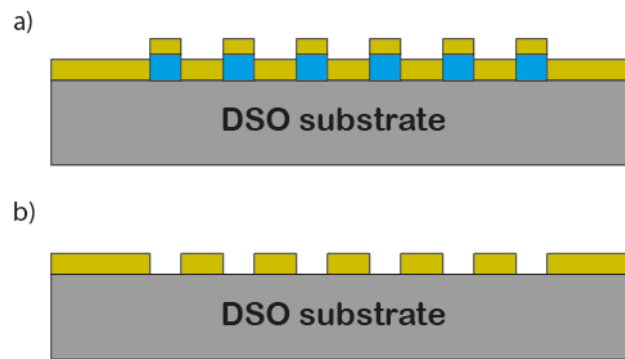


Figure 3.2 A schematic illustration of the fabrication process of the ZnO mask. The ink (the ZnO solution) is applied to the PDMS stamp (a), which is then applied on the substrate (b). After hardening, the stamp is removed, leaving behind the ZnO mask (c).

### 3.3 PLD growth of SrRuO<sub>3</sub> nanowires

After the mask creation, a thin layer of SrRuO<sub>3</sub> was deposited on top of the sample using PLD. For the deposition a 248 nm wave length KrF excimer laser was used at an energy density of 2.1 J/cm<sup>2</sup> on a surface area of 1.8 mm<sup>2</sup>. A pre-ablation step was included to clear the SrRuO<sub>3</sub> target of impurities. The target was pre-ablated for 6 minutes with a pulse frequency of 5 Hz. With a substrate temperature of 670 °C the ablation took place for 16 minutes with a pulse frequency of 1 Hz, under a pressure of 0.3 bar with a gas flow of 50% O<sub>2</sub> and 50% Ar. The deposition created a SrRuO<sub>3</sub> layer on top of the ZnO structures, see

figure 3.3a. The ZnO mask was then removed by putting the substrate in an ultrasonic bath, in 0.01wt% HCl solution for 5 minutes, then twice in water for 2 minutes. After dipping the substrate in ethanol it was blowdried with a N<sub>2</sub> gun. After this process only the SrRuO<sub>3</sub> structures were left, see figure 3.3b. On some samples a second and third SrRuO<sub>3</sub> layer was deposited to investigate the further growth mechanics.



**Figure 3.3** A schematic illustration of the growth of SrRuO<sub>3</sub>. A layer of SrRuO<sub>3</sub> (dark yellow) is deposited on top of the DyScO<sub>3</sub> substrate with the ZnO mask (blue) (a). The ZnO mask is then etched away using a HCl solution (b).

## 4 Results and discussion

### 4.1 DyScO<sub>3</sub> substrate treatment

The DyScO<sub>3</sub> substrates needed treatment before they could be used to grow SrRuO<sub>3</sub> (see section 3.1). The substrates were annealed for 4 hours at 1000°C. In figure 4.1 an AFM image of a substrate is shown. The step structure is clearly seen, with a step height equal to the lattice constant of 3.932 Å.

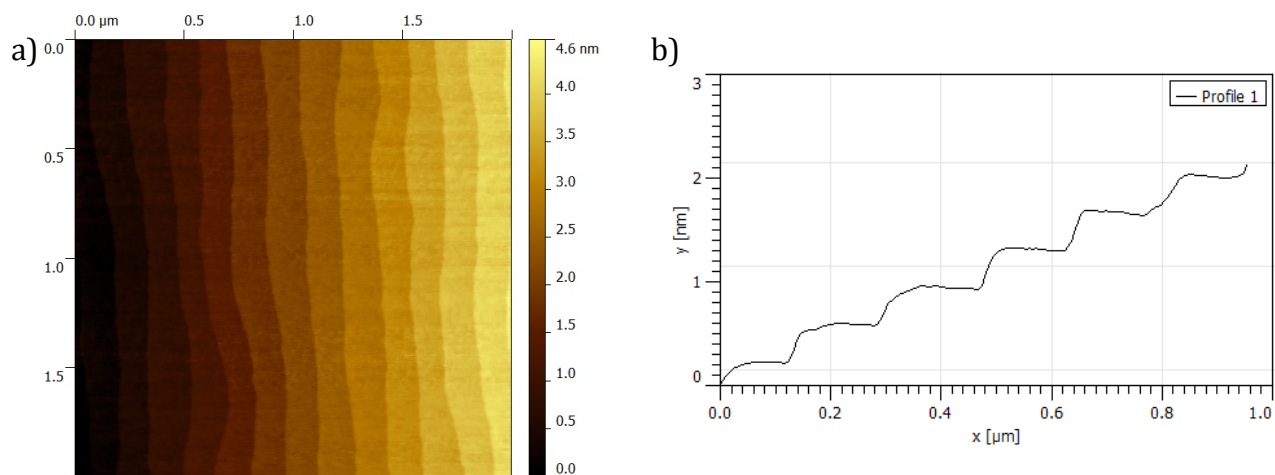


**Figure 4.1** AFM image of a DyScO<sub>3</sub> substrate after annealing for 4 hours at 1000 °C (a), and the height profile (b).

To make the substrates single terminated, the substrate was immersed in NaOH after annealing. Some substrates were roughened using HF to allow a faster chemical reaction. The difference in structure between substrates which were roughened and substrates which were not roughened can be seen in figure 4.2. The roughening has a pronounced effect on the surface topography.

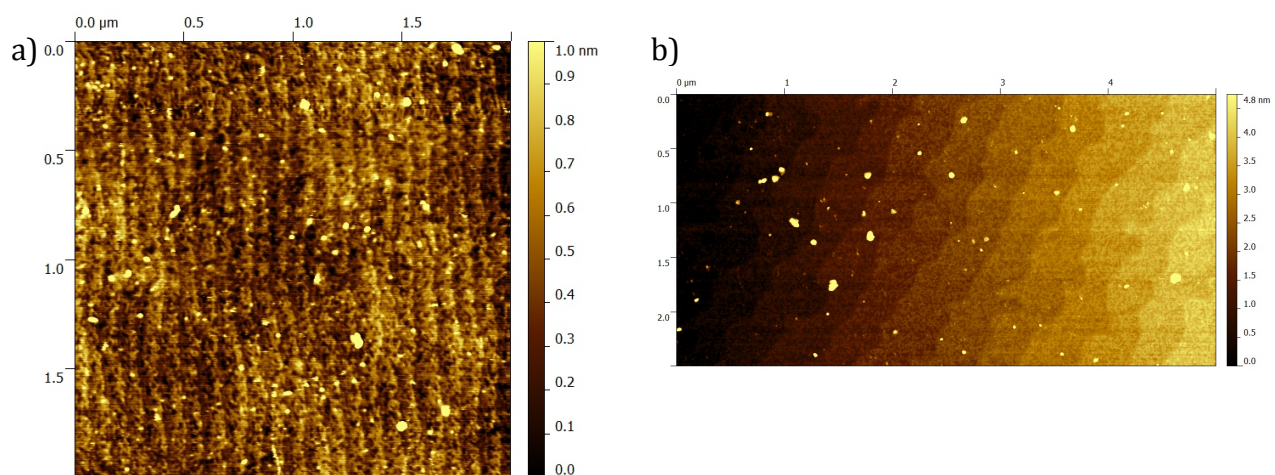


**Figure 4.2** AFM images of a DyScO<sub>3</sub> substrate treated with NaOH and HF (a), and a DyScO<sub>3</sub> substrate treated with only NaOH (b)

## 4.2 SrRuO<sub>3</sub> growth on DyScO<sub>3</sub>

SrRuO<sub>3</sub> was grown on DyScO<sub>3</sub> without any mask. The resulting films were not smooth, but full of trenches. Two identical depositions were performed with the deposition settings described in section 3.3, but one with the roughening procedure and one without. The results at 0.3 mbar were similar, as can be seen in figure 4.3a and b. The surfaces of these samples showed deep trenches, and although the sample conducted electricity, when nanowires are made out of these structures it is highly probable that the transport of electrons through the material is obstructed by the trenches, since they will cut the nanowires off if the trenches reach the DyScO<sub>3</sub> substrate.

Interestingly, the sample from figure 4.3b showed smooth SrRuO<sub>3</sub> growth in the corner of the sample, as can be seen in figure 4.3c. This change from a surface full of trenches to an almost smooth terrace surface was gradual and was only observed in this sample. An explanation can at this point not be given, but it might be related to a difference in deposition temperature between the corner and the center of the sample, if the contact between the heater and sample was not equal over the whole sample.

A deposition was performed at a lower deposition pressure of 0.010 mbar instead of 0.3 mbar. The results of this deposition can be seen in figure 4.3d. The surface is reasonably smooth, with height variations around 2 nm. There are no trenches, and no step structure can be seen which should be the case in an ideal layer-by-layer growth.

These samples indicate that even though we used methods that were used successfully in previous research, it does not give the same results. This might be a problem related to the chemical terminations of the substrates.

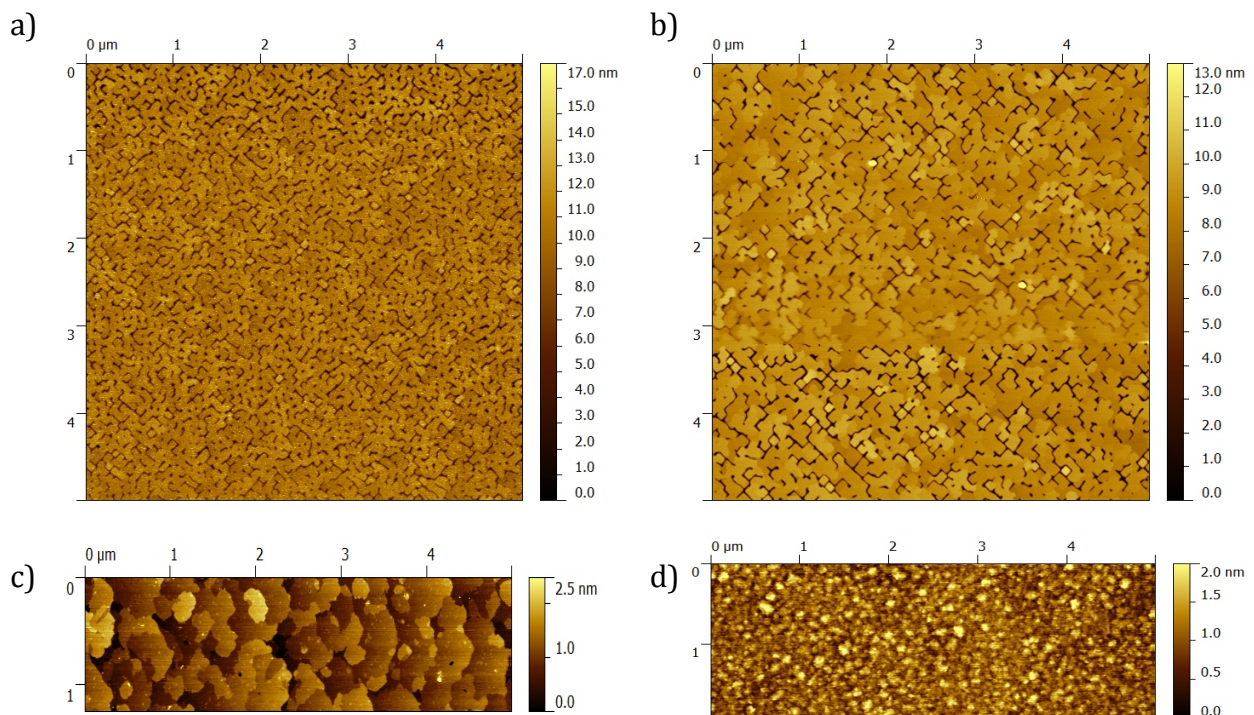


**Figure 4.3** AFM images of SrRuO<sub>3</sub> growth on: HF-treated DyScO<sub>3</sub> at 0.3mBar (a), non-HF-treated DyScO<sub>3</sub> at 0.3mBar (b), non-HF-treated DyScO<sub>3</sub> at 0.3mBar scanned in the corner of sample (c), and HF-treated DyScO<sub>3</sub> at 0.01mBar (d).

### 4.3 ZnO mask fabrication on Si

A ZnO mask was fabricated on silicon. Figure 4.4 shows AFM images of the height of the mask after three stages of fabrication on Si. The damage on the structures near the edge of the image was deliberately created to find the same spot on the sample after every processing step, so a good comparison could be made.

The initial structures had a height of around 90 nm, and after the ultrasonic bath and annealing a height of around 20 nm, as can be seen in figure 4.4d. The structures were nearly without defects and unwanted particles. While the height of the structures was decreased by a factor 4, the width only decreased by a factor of 2. This is due to the clamping effect the substrate has on the ZnO. After annealing the tops of the structures were nearly flat, which was very different from the structures before annealing, the reason for this is unknown.

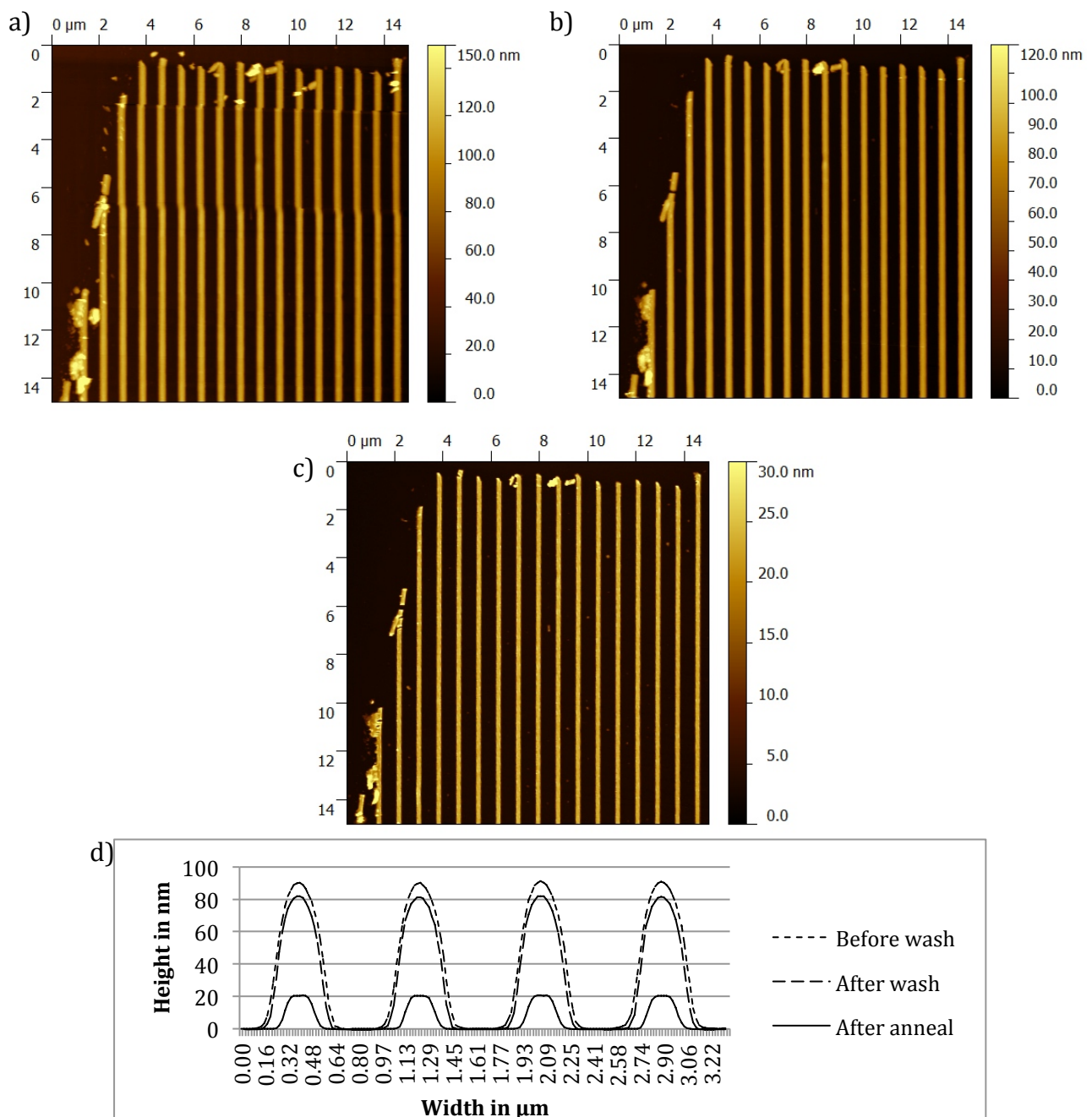


**Figure 4.4** AFM images of the ZnO mask on Si before (a) and after (b) washing the sample in an ultrasonic bath, after annealing (c), and the height profiles of these steps (d).

#### 4.4 ZnO mask fabrication on DyScO<sub>3</sub>

For making the ZnO mask on DyScO<sub>3</sub> the same procedure was followed as for fabricating the mask on Si. This section shows the process for three samples, all three substrates were roughened using HF and treated to obtain single termination. The ZnO structures that resulted after soft-lithographic patterning were significantly lower on DyScO<sub>3</sub> than on Si. Figure 4.5a shows an AFM image of the ZnO mask on sample 1 after annealing, and figure 4.5b shows the height profile of the structure. Aside from the many particles, the structures on sample 1 were reasonably smooth. The average height was around 7 nm.

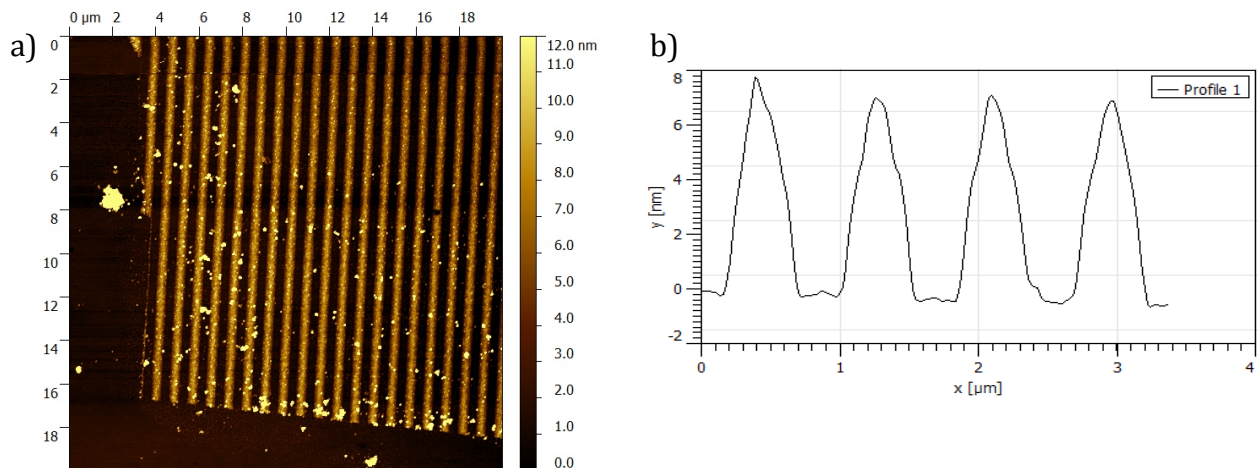


Figure 4.5 AFM image of ZnO mask on DyScO<sub>3</sub> after annealing (a), and the height profile (b). (Sample 1)

Sample 2 had a much cleaner surface, with almost no particles and a smoother surface than sample 1. The feature height was around 17nm. An AFM picture and the height profile can be seen in figure 4.6.

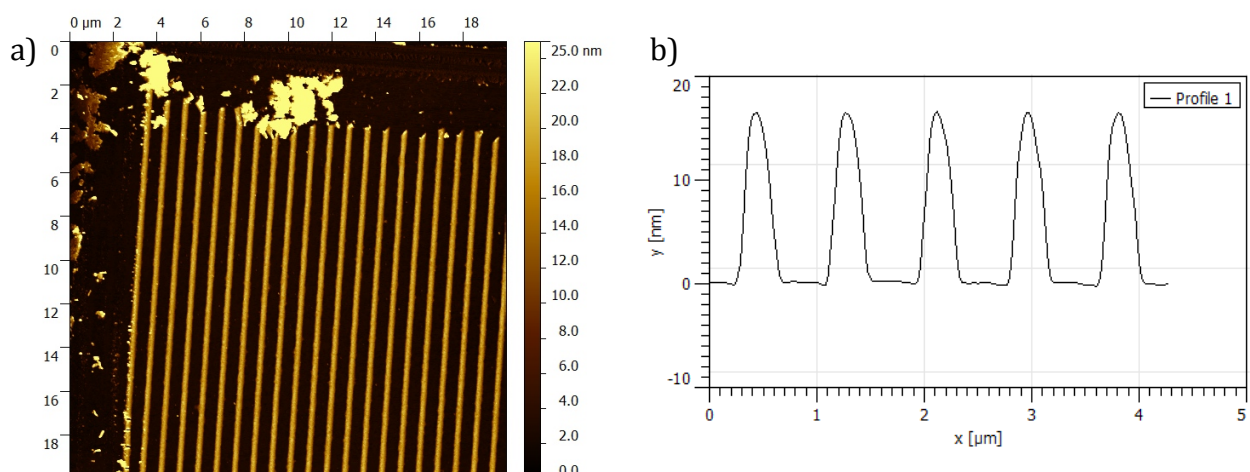
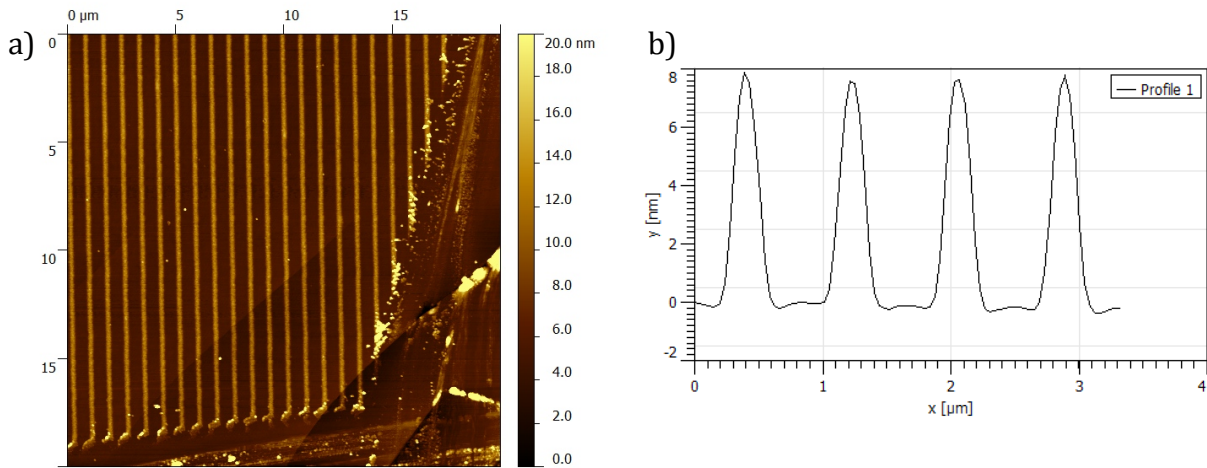


Figure 4.6 AFM image of ZnO mask on DyScO<sub>3</sub> after annealing (a), and the height profile (b). (Sample 2)

Sample 3 had clean structures with a height around 8nm. Figure 4.7 shows an AFM image and the height profile of sample 3.



**Figure 4.7** AFM image of ZnO mask on DyScO<sub>3</sub> after annealing (a), and the height profile (b). (Sample 3)

Although the mask height on Si was nearly constant around 20nm, the mask height on DyScO<sub>3</sub> varied between the different samples, but it was generally lower than the masks on Si. This might be because of differences in surface chemistry of the substrates.

#### 4.5 Growth of SrRuO<sub>3</sub> on the ZnO mask

A 16 minute deposition at 1 Hz resulted in a SrRuO<sub>3</sub> film of around 10nm. A smooth film was found on sample 1, of which an AFM scan can be seen in figure 4.8a and the height profile can be seen in figure 4.8b. The step edges of the

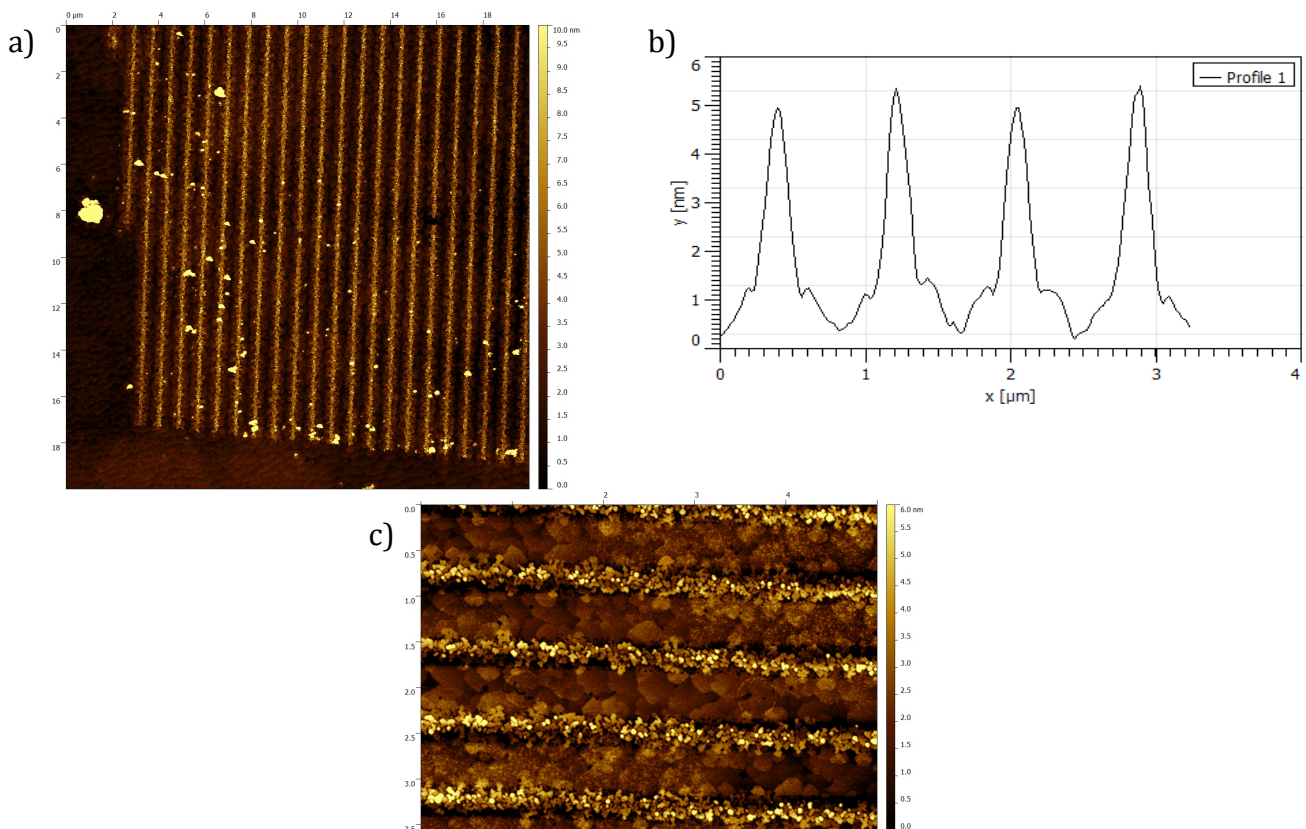


**Figure 4.8** AFM image of SrRuO<sub>3</sub> growth on sample 1 (a), the height profile (b), and a scan in the direction of the structures (c).

substrate can still be seen through the SrRuO<sub>3</sub> layer (figure 4.8c). The low pattern height is not ideal, but this sample proved that smooth SrRuO<sub>3</sub> growth was possible on DyScO<sub>3</sub>. A deep trench in between the structures can be seen in both figures 4.8a and b. This could be a scan artifact, or might indicate that the SrRuO<sub>3</sub> film grew towards the ZnO mask during deposition.

From this scan two different growth mechanisms can be distinguished. In between the structures atomically smooth material was observed with clear step edges, indicating two-dimensional (step-flow) growth. On top of the ZnO structures a rougher film was observed, so three dimensional island growth was a possible mechanism. A first layer of islands was deposited, after which the new SrRuO<sub>3</sub> tended to grow on top of the SrRuO<sub>3</sub> islands instead of on top of the ZnO. Because the islands could grow in different directions, they would not join in a single crystalline structure, which was why smooth growth was not achieved. Since the ZnO mask would be etched away the SrRuO<sub>3</sub> layer on this mask would also go away, so only the growth in between the structures was of importance.

Figure 4.9 shows sample 2 after the deposition of SrRuO<sub>3</sub>. The surface in between the ZnO structures was not smooth, indicating (partial) island growth. A close look at that area (figure 4.9c) showed similar morphology as found in figures 4.8c, with islands on top. Similar as for sample 1, sample 2 showed rough growth on top of the ZnO mask.

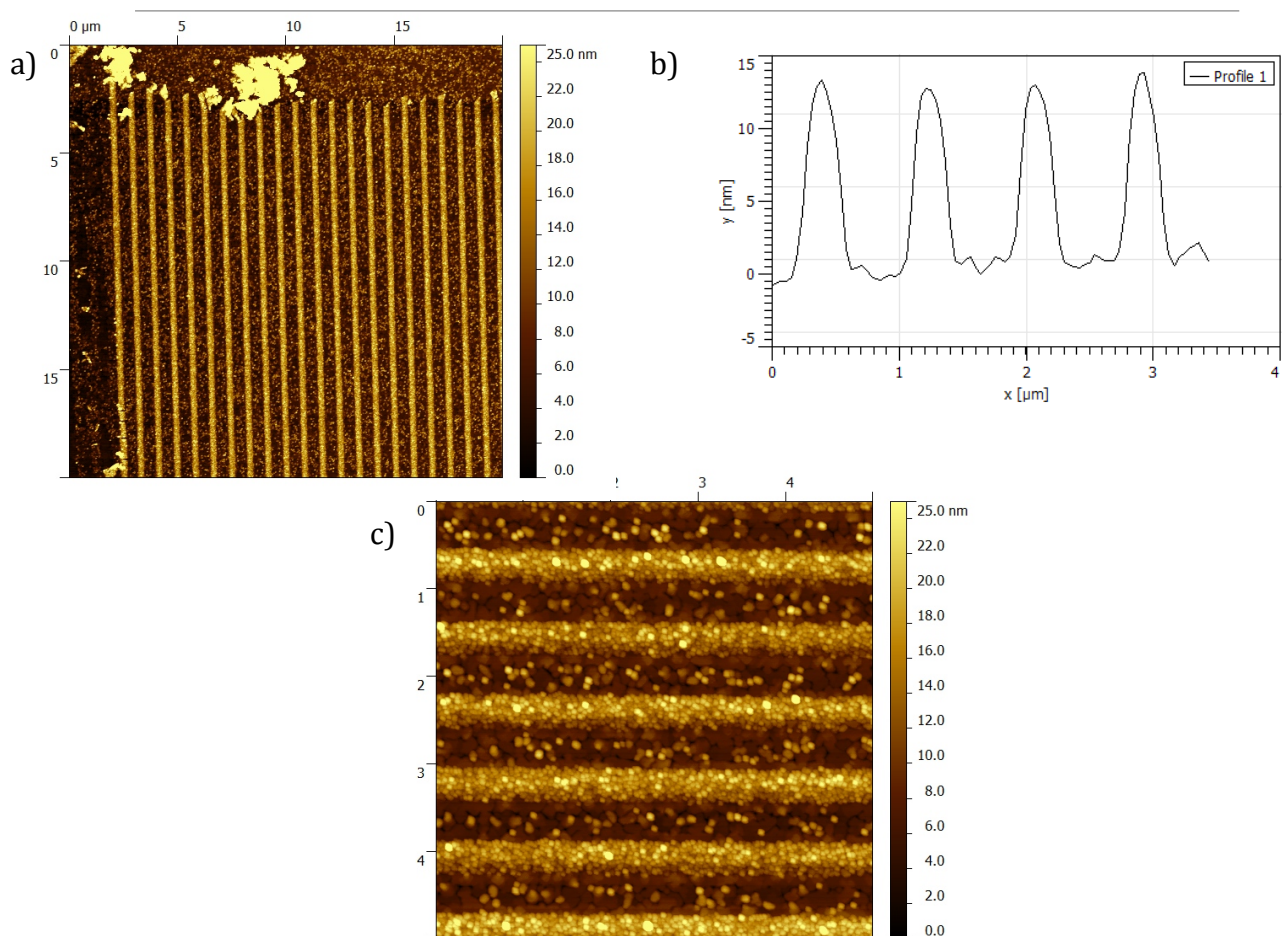


**Figure 4.9** AFM image of SrRuO<sub>3</sub> growth on sample 2 (a), the height profile (b), and a scan in the direction of the structures (c).

Figure 4.10 shows the AFM scan and height profile of sample 3 after the deposition of SrRuO<sub>3</sub>. The surface was not smooth, consisting of dense islands, similar to those on top of the ZnO lines on sample 1 and 2. Just as with sample 2, the area between the ZnO structures also showed unwanted islands, though to a much higher degree than sample 2. Because of the island growth in between the structures it was impossible to tell how high the structures were compared to the DyScO<sub>3</sub> substrate. For unknown reasons, the material on top of the structures seemed lower than that in between the structures, which was very different compared to the other samples. The results of this sample were very different from the other two samples. This might have had to do with difficulties in making the substrate single terminated, or some other surface chemistry effect.

Using a 0.01 wt% HCl solution the ZnO mask was etched away and the top

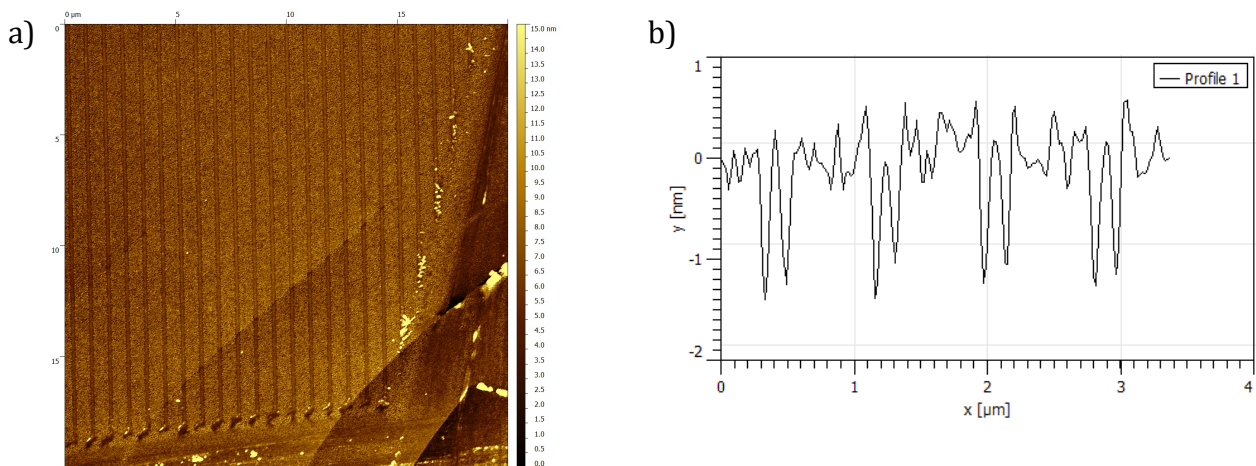


**Figure 4.10** AFM image of SrRuO<sub>3</sub> growth on sample 3 (a), and the height profile (b).

SrRuO<sub>3</sub> layer could be rubbed off. Due to the thick SrRuO<sub>3</sub> layer a considerable amount of force was necessary to rub away all ZnO traces, the impact of this treatment can be seen by the lack of step edges on the surface of sample 1 (see figure 4.11a). The surface of sample 2 was destroyed in this process to the point that it became unusable.

Figure 4.11b shows the height profile of the nanowires on sample 1. Since the ZnO layer was etched away, the height profile should show the inverse of figure 4.5b. This would mean that the structures should be narrower at the base than at the top. However, due to the nature of the AFM this could not be measured. A structure height of 6nm was measured. The top of the structures

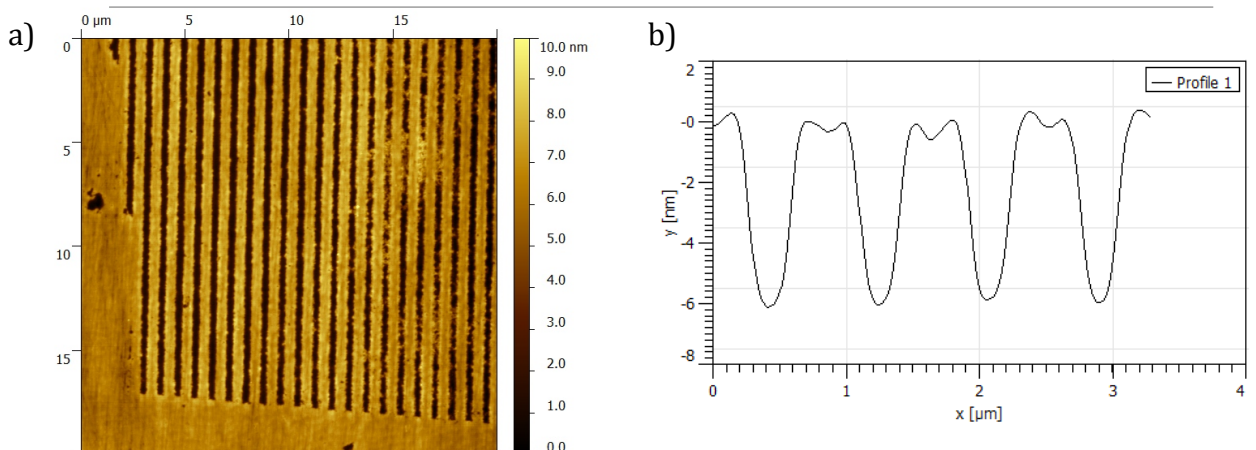


**Figure 4.11** AFM image of the SrRuO<sub>3</sub> nanowires on sample 1 after HCl etching (a), and the height profile (b).

was not flat, which could also be seen in between the ZnO mask in figure 4.8b.

After the rubbing process to remove the ZnO mask, the nanowires on sample 3 still showed the same rough surface as before (figure 4.12), this meant that either the top layer of the structure was not rubbed off, or that the roughness was not only on the surface, but might have gone further into the structure. Since the top layer of sample 1 was easily rubbed off it is reasonable to assume that the latter case is true. A structure height of around 5 nm can be seen. In between the nanowires a structure could be seen, which might be due to a scanning error or some other unknown reason. Therefore the structure height is not certain.

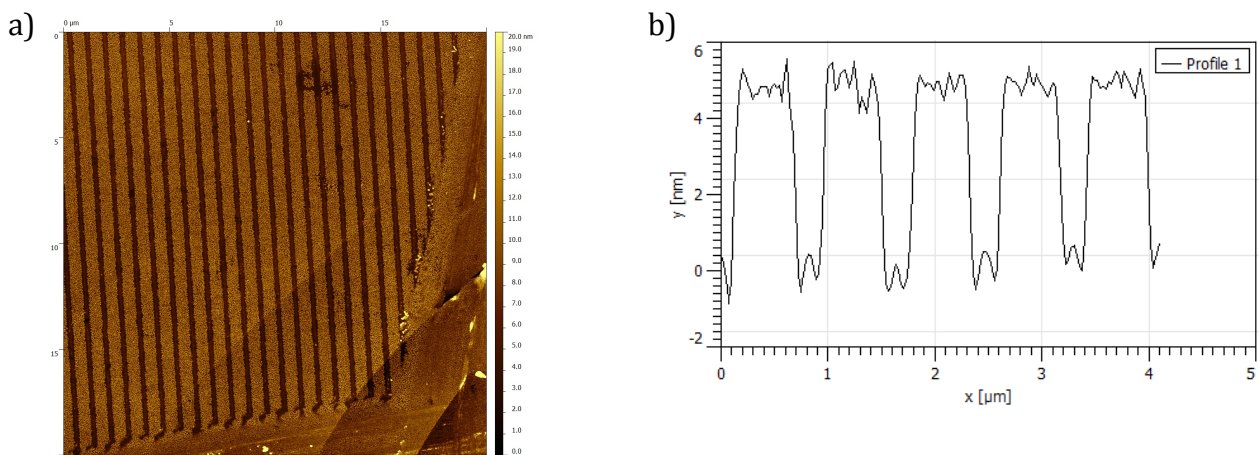


**Figure 4.12** AFM image of the SrRuO<sub>3</sub> nanowires on sample 3 after HCl etching (a), and the height profile (b).

#### 4.6 Second and third SrRuO<sub>3</sub> deposition

After depositing a first layer of SrRuO<sub>3</sub>, more layers of SrRuO<sub>3</sub> were deposited on top of the old layer to study the growth mechanics. A second layer was deposited on top of sample 1, for a total of 300 pulses, which resulted in a deposition thickness of around 3nm. Figure 4.13 shows the result. The result looked very similar to the sample after the first deposition (figure 4.11), indicating a smooth 2D layer-by-layer growth. The profile, showed a decrease in structure height of around 2.5 nm. This was only 0.5nm less than the expected deposition thickness.

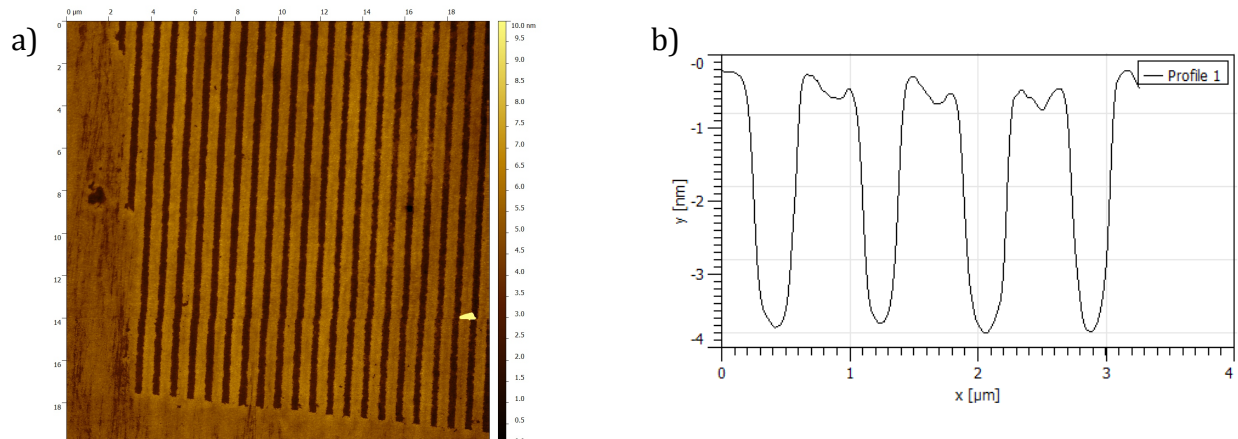


**Figure 4.13** AFM image of the second SrRuO<sub>3</sub> deposition on sample 1 (a), and the height profile (b).

Therefore most of the  $\text{SrRuO}_3$  growth seemed to have taken place on top of the  $\text{DyScO}_3$  in between the existing structures, though this might only seem this way because the AFM tip might not have reached the bottom.

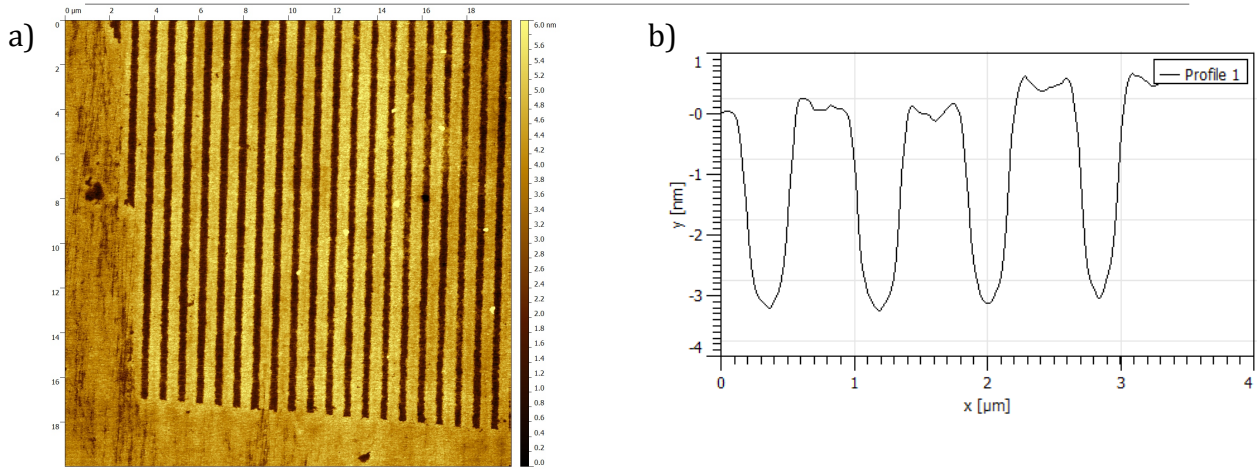


**Figure 4.14** AFM image of the third  $\text{SrRuO}_3$  deposition on sample 1 (a), and the height profile (b).

A third deposition of 250 pulses was performed. The results are shown in figure 4.14. A slight decrease of structure height of about 0.5 nm was observed. The new  $\text{SrRuO}_3$  layer seemed to have grown evenly across the whole surface, except for the small decrease in height, which could have been due to the

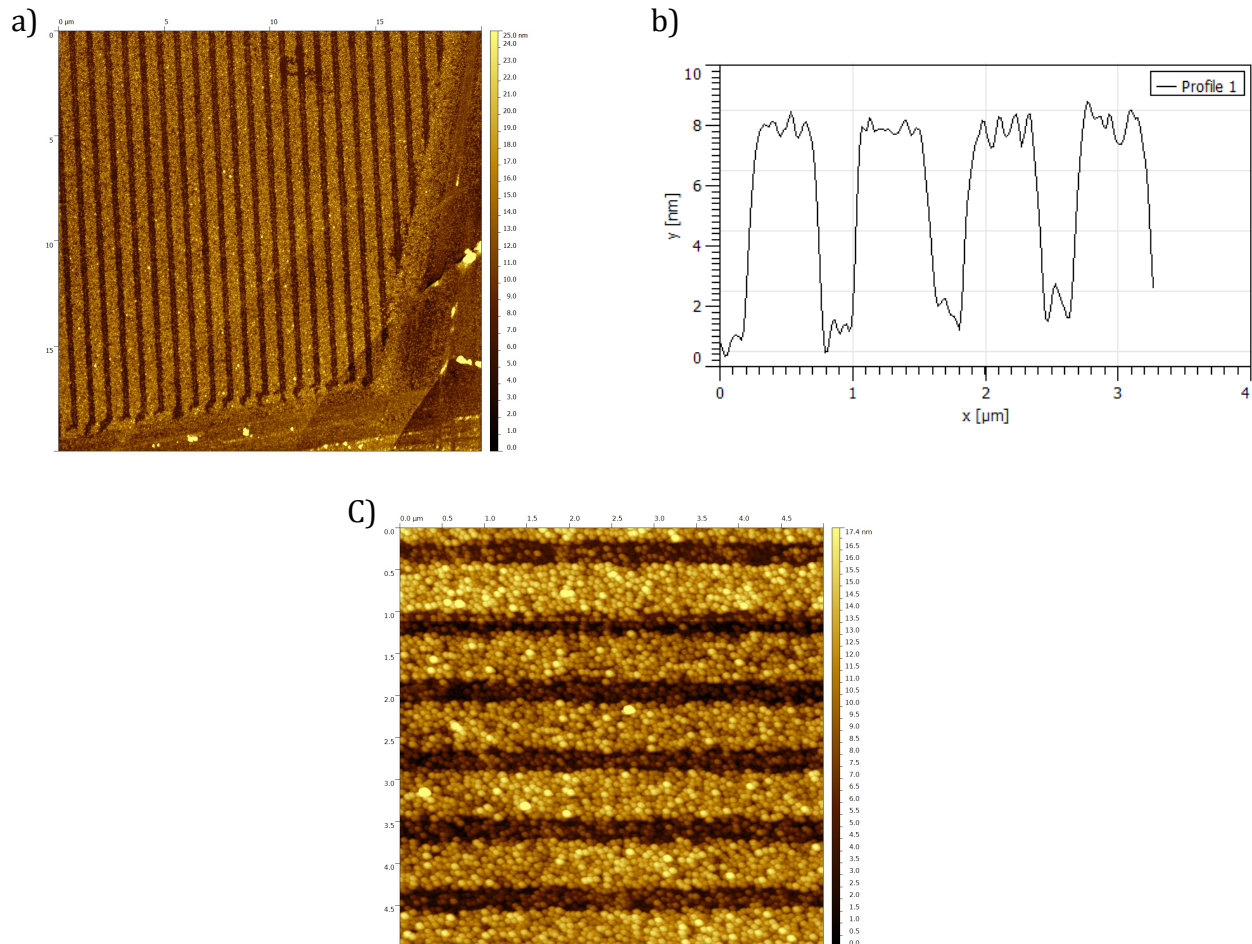


**Figure 4.15** AFM image of the second  $\text{SrRuO}_3$  deposition on sample 3 (a), the height profile (b), and a closer look at the structures (c).

annealing effect of the heater, since the surface energy of the structures is higher than the surface energy of flat films.

A second SrRuO<sub>3</sub> layer was grown on sample 3. The result can be found in figure 4.15. Contrary to what was observed at sample 1, the structure height on sample 3 had increased with around 3 nm. A closer look at the sample (figure 4.15c) shows island growth on and in between the nanowires. However, since the height shown in figure 4.12b could be due to a scan artifact it is uncertain if there is an height increase or not.

#### 4.7 Electrical analysis of the SrRuO<sub>3</sub> nanowires

Using conductive AFM the electrical conductivity of sample 1 was analyzed. Figure 4.16 shows the result. The conductivity was measured some hundreds of micrometers from the edge of the silver paste. This showed that conductivity could be achieved over long distances using these structures as nanowires.

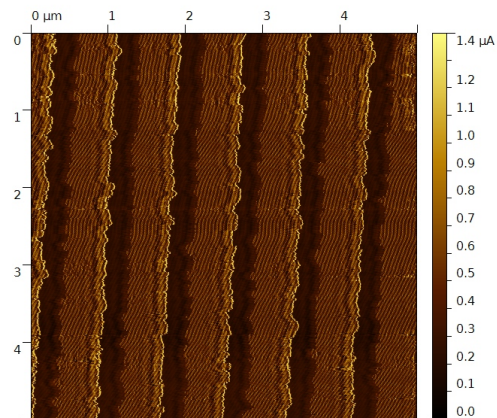


**Figure 4.16** C-AFM scan of sample 1.

## 5 Conclusion and recommendations

There was a relatively low success rate in the creation of SrRuO<sub>3</sub> nanowires. There were several different mechanics in play that could hinder the whole process of creating the nanowires. The high failure rate might have been partly due to the inconsistency in achieving a single terminated substrate, leading to a SrRuO<sub>3</sub> growth with trenches as can be seen in figures 4.4a and b.

The creation of ZnO masks on silicon gave consistent results with a pattern height around 20 nm, but problems were encountered when the same method was used on DyScO<sub>3</sub>. In many cases the mask would not be transferred properly to the substrate, or there might have been residual ZnO in between the ZnO structures. Most of these faults were hard to detect until after the SrRuO<sub>3</sub> deposition, leading to a considerable amount of unusable samples.

The deposition of SrRuO<sub>3</sub> on the DyScO<sub>3</sub> gave inconsistent results. When a SrRuO<sub>3</sub> film was deposited on a sample without mask, a relatively smooth film with deep trenches was observed. But as indicated by figures 4.3b and c, a difference in contact between the substrate and the PLD heater could have led to a temperature difference across the substrate, leading to different growth mechanics.

The SrRuO<sub>3</sub> growth on DyScO<sub>3</sub> in between the mask seemed to be very different from the growth on top of the ZnO mask. The latter led to the formation of islands with high peaks, while the former showed inconsistent results. Sample 1 and 2 were relatively smooth, with some islands on sample 2. Islands similar to those on the ZnO structures were observed on sample 3, which could have been due to a residual ZnO layer or some other surface chemistry effect.

The deposition of the second and third SrRuO<sub>3</sub> layers followed similar growth mechanics as the underlying layers. In both samples growth was observed between the nanowires. On sample 1 the growth seemed to mainly take place in between the nanowires, resulting in lower structure height, while on sample 3 the structures increased in height, which indicates that the SrRuO<sub>3</sub> mainly grew on top of the nanowires. This difference may be due to the difference in growth mechanics between the two samples, but it is uncertain if the AFM tip always reached the bottom of the structures.

Section 4.7 shows that the used method allows for the creation of long nanowires which can, for example, be used in nanoelectronics as electrodes.

More research needs to be done on the production of the nanowires, since the current method had a too low success rate. A better method to create stamps may be developed, with a higher success rate on DyScO<sub>3</sub>. ZnO complexes with different concentrations or completely different solutions may be tried. Since the deposition of SrRuO<sub>3</sub> gave inconsistent results, little research could be done to further understand the growth mechanics. Different PLD settings may be tried to increase the success rate, such as different temperatures and different pressures.

Finding good methods to obtain single terminated DyScO<sub>3</sub> substrates and obtain consistently good structures is advised before any further research can be performed on the growth mechanics of a second or third layer.

## 6 Acknowledgements

First of all I would like to thank Maarten Nijland. Not only did he guide me throughout the whole process and did he help me with anything he could, he was also incredibly patient and understanding of my situation and the fact that it took so long for me to finish this assignment. Thank you!

Second of all I would like to thank my parents for their financial and moral support throughout my studies. Without their help I probably never would have reached this point.

I would like to thank the University of Twente and the Inorganic Materials Science (IMS) group for giving me the opportunity to do this assignment, and for financing the research. Especially thanks to all the people of IMS who were always ready to answer questions and help me with anything I needed.

And of course everyone else whom I did not name, but in some way helped me along.

Thanks!

## 7 References

- [1] J.G. Bednorz and K. A. Müller. Possible high  $T_c$  superconductivity in the Ba-La-Cu-O system. *Zeitschrift für Physik B Condensed Matter*, 64:189–193, 1986.
- [2] Jing Xia, W. Siemons, G. Koster, M. R. Beasley, and A. Kapitulnik. Critical thickness for itinerant ferromagnetism in ultrathin films of  $\text{SrRuO}_3$ . *Physical Review B (Condensed Matter and Materials Physics)*, 79(14):140407, 2009.
- [3] M. Dawber, K.M. Rabe, and J.F. Scott. Physics of thin-film ferroelectric oxides. *Reviews of Modern Physics*, 77:1083–1130, October 2005.
- [4] G. Koster, L. Klein, W. Siemons, G. Rijnders, J. S. Dodge, C. Eom, D. H. A. Blank and M. R. Beasley. Structure, physical properties, and applications of  $\text{SrRuO}_3$  thin films. *Reviews of Modern Physics*, 84:253-298, 2012.
- [5] B. Kuiper, J. L. Blok, H. J. W. Zandvliet, D. H. A. Blank, G. Rijnders and G. Koster. Self-organization of  $\text{SrRuO}_3$  nanowires on ordered oxide surface terminations. *MRS Communications*, 2011.
- [6] K. M. Rabe, C. H. Ahn and J. M. Triscone. *Physics of Ferroelectrics, A Modern Perspective*. Springer 2007 ISBN 978-3-540-34590-9.
- [7] B. Kuiper, Master thesis, University of Twente, 2009.
- [8] J. E. Kleibeuker, B. Kuiper, S. Harkema, D. H. A. Blank, G. Koster and G. Rijnders. Structure of singly terminated polar  $\text{DyScO}_3$  (110) surfaces. *Physical Review B*, 85:165413, 2012.
- [9] J. Broekmaat, Ph.D. thesis, University of Twente, 2008.
- [10] R. Eason. *Pulsed laser deposition of Thin Films*. Wiley, 2007, ISBN 978-0-471-44709-2.
- [11] J. E. Kleibeuker, G. Koster, W. Siemons, D. Dubbink, B. Kuiper, J. L. Blok, C. H. Yang, J. Ravichandran, R. Ramesh, J. E. ten Elshof, D. H. A. Blank and G. Rijnders. Atomically defined rare-earth scandate crystal surfaces. *Adv. Funct. Mat*, 20, 3490-3496, 2010.
- [12] A. Padilla and A. Vazquez. Synthesis and characterization of polyacrylic acid-zinc oxide composites. *J. Mater. Res.*, Vol. 6, No. 11, Nov 1991.
- [13] A. Padilla and A. Vazquez. Porosimetry studies on polyacrylic acid – ZnO cements. *Journal of Materials Science: Materials in Medicine* 1 (1990) 154-156.